ANN-enabled Gain Prediction and Optimization in Dual-band SIW Antenna Design for 5G Networks

Md Mahabub Alam, Md Raihanul Islam Tomal, Ahmad Afif Mohd Faudzi, and Nurhafizah Abu Talip Yusof

Universiti Malaysia Pahang Al-Sultan Abdullah, Pahang, Malaysia

https://doi.org/10.26636/jtit.2026.1.2424

Abstract — Artificial neural networks (ANNs) help improve antenna design process by enabling adaptive optimization strategies that address important challenges in 5G wireless systems, including signal interference, limited coverage, and high user density. This study presents an AI-assisted design methodology for a compact dual-band substrate integrated waveguide (SIW) antenna optimized for 5G operation at 28 and 38 GHz. The antenna is implemented on a Rogers RT/Duroid 5880 substrate using a novel slot configuration with strategically positioned vias to enhance radiation characteristics. The fabricated prototype achieves gains of 8.05 dBi at 28 GHz and 7.89 dBi at 38 GHz, with fractional bandwidths of 6.41% (27.491 – 29.277 GHz) and 1.81% (37.496 – 38.179 GHz), while maintaining a return loss below –10 dB across both operating bands. The pivotal contribution of this work is the development of an ANN-based predictive model capable of accurately estimating antenna gain and radiation efficiency from main parameters such as slot dimensions, via size and feedline width. The proposed model demonstrates excellent predictive accuracy, achieving mean squared error values in the range of 0.00 to 0.001 for gain prediction and 0.018 to 0.066 for radiation efficiency estimation. This AI-driven framework significantly reduces design iterations, computational overhead, and prototyping requirements, offering an automated framework for efficient antenna development in next-generation 5G communication networks.

Keywords — 5G, ANN, gain prediction, machine learning, mmWave, SIW antenna

1. Introduction

To cope with limitations, including restricted bandwidth, high latency, substantial power consumption, limited scalability for the Internet of Things (IoT), and security vulnerabilities, 5G networks utilize three primary frequency bands including sub-6 GHz, millimeter wave (mmWave), and unlicensed bands [1], [2]. The mmWave spectrum, particularly the 28 and 38 GHz bands, is most important, as it offers unprecedented data rates and ultra-low latency required for next-generation wireless applications [3]. However, realizing this potential remains challenging due to severe propagation impairments at high frequencies, including increased loss of free space path and atmospheric attenuation, especially in dense urban environments [4].

To address these challenges, researchers have increasingly focused on developing compact, low-cost, and high-performance antennas for 5G networks, particularly of the microstrip patch type [5]. While simple and easily integrated, their performance at mmWave frequencies is limited by narrow bandwidth, low efficiency, and insufficient gain [6]. The antenna arrays offer a potential solution to these challenges, but unfortunately they come with considerable drawbacks, such as greater design complexity, increased size, and higher cost [7], [8].

In such a context, the substrate integrated waveguide (SIW) technology is a promising alternative, as it combines the high performance of conventional waveguides with the compactness and manufacturability of microstrip structures [9], [10]. SIW-based antennas support low-loss, wideband operation, and planar integration, making them particularly suitable for dual-band 5G applications in the 28 and 38 GHz spectrums [11], [12].

SIW slot antennas further enhance design flexibility through strategically positioned slots, though challenges remain in achieving wide bandwidth, efficient dual-band performance, and adaptive beam control at mmWave frequencies [13], [14]. Although full-wave electromagnetic simulators such as CST Microwave Studio and HFSS provide high accuracy for SIW slot antenna analysis, their reliance on dense meshing and iterative computations results in high computational cost and slow convergence [15], [16].

On the contrary, artificial neural networks (ANNs) enable fast antenna design by automating parameter optimization and accurately predicting pivotal performance metrics, such as gain, bandwidth, and radiation efficiency, without time-consuming prototyping [17].

This study bridges that gap by introducing a novel dual-band SIW antenna optimized for 28 and 38 GHz 5G operation [18].

The contributions of the proposed method are as follows:

- novel dual-band SIW antenna design with optimized slotted structures that achieve dual-band operation at 27.83 GHz and 37.81 GHz,
- integration of ANN predictive modeling for antenna performance estimation (gain, bandwidth, radiation efficiency),

which reduces the dependency on time-consuming CST simulations,

- comprehensive data set generation and parametric optimization which supports accurate ANN training and predictive capabilities.

2. Slotted SIW Microstrip Patch Antenna

The design process involves a series of stages, from the definition of material specifications to the refinement of antenna parameters, with the goal of achieving optimal performance in terms of gain, bandwidth, and efficiency. Figure 1 presents the workflow used to design and optimize the proposed slotted SIW antenna. The process begins by selecting the target operating bands and defining the substrate properties and design variables.

A parametric analysis is then performed by varying the slot dimensions (L_1, L_2, L_3, and W_1, W_2, W_3). Then, the antenna's performance is evaluated in terms of return loss, VSWR, gain, directivity, bandwidth, efficiency, and surface current distribution. If the performance satisfies the design targets, the results are finalized and compared with previously reported work. Otherwise, optimization is carried out to refine the structure.

The resulting data are statistically examined using ANOVA, and when a significant p-value ($\leqslant 0.05$) is obtained, a regression model is developed to further analyze performance trends. The adequacy is verified and, if necessary, additional optimization is performed. Once validated, the final design is confirmed using CST simulations and benchmarked against the published literature.

This methodology is scalable across multiple frequency bands (S, X, Ku, K, and Ka) by redefining the operating frequency and adjusting design parameters such as slot length, via diameter, and waveguide width relative to wavelength. Parametric modeling, supported by ANOVA and regression analysis, ensures accurate performance prediction under different geometric and material configurations, enabling robust and adaptable antenna optimization.

2.1. Evolution of the Dual-band SIW Antenna

This section presents the development of a dual-band SIW antenna through three design iterations, all modeled and optimized in CST. As shown in Fig. 2, each design is based on a compact 27 × 7.5 mm structure using a Rogers RT/Duroid 5880 substrate with relative permittivity of $\varepsilon_r = 2.2$ and thickness $h = 0.254$ mm. Antenna 1 introduces a 9 × 0.7 mm longitudinal slot and metallic vias forming the SIW sidewalls, together with a 3.50 × 0.37 mm feedline for impedance matching. Antenna 2 adds a 3.1 × 0.7 mm transverse slot to achieve dual-band operation. The final design, antenna 3, incorporates two longitudinal slots (9 × 0.7 mm and 7.7 × 0.7 mm), along with the transverse slot, to further enhance performance.

The S_{11} analysis indicates that antenna 1 provides a single resonance at 27.82 GHz with a return loss of –21.71 dB,

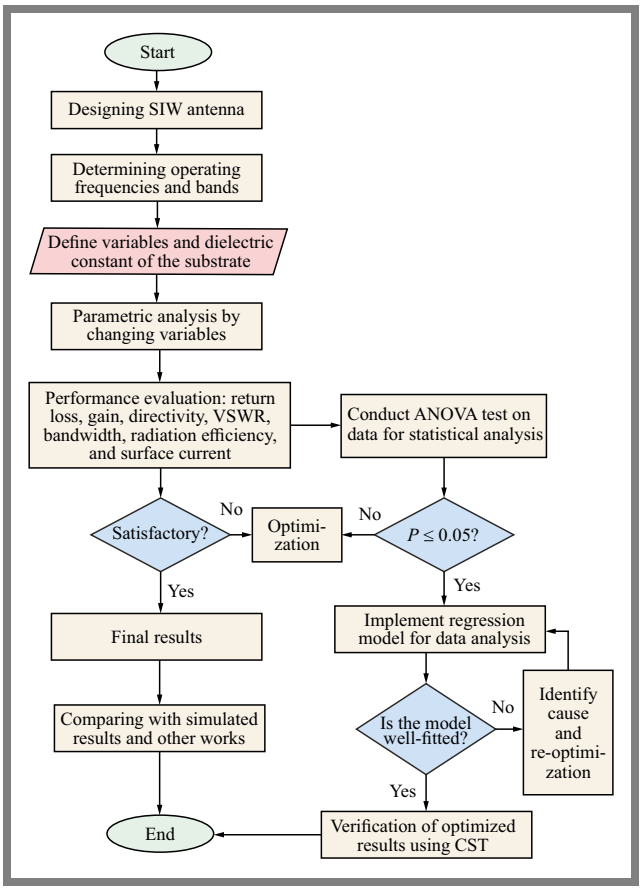

Fig. 1. Flowchart of slotted SIW antenna design and developed ANN model details.

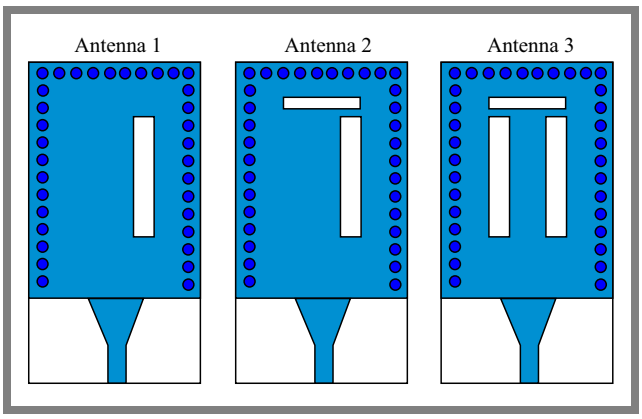

Fig. 2. Evolution of the design from single to triple-slot SIW antenna (no. 3).

as shown in Fig. 3. Antenna 2 introduces dual resonances at 28.29 GHz (–21.19 dB) and 37.87 GHz (–33.7 dB), confirming effective dual-band operation. The optimized design shown as antenna 3 exhibits deeper and more stable resonances at 27.83 and 37.81 GHz, with an effective operating range extending from 26 to 40 GHz.

This demonstrates a substantial improvement in bandwidth and impedance matching compared to the previous designs. These results clearly show that incorporating the second longitudinal slot enhances coupling and current distribution,

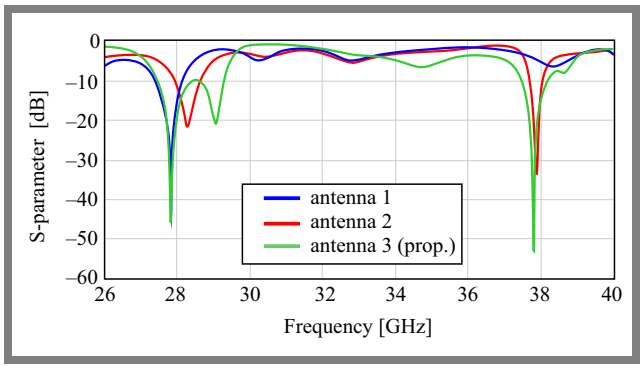

Fig. 3. S_{11} analysis and optimization for antennas 1 – 3.

leading to stronger resonances and superior dual-band performance.

2.2. Proposed Antenna Configuration

The proposed antenna incorporates a substrate-integrated waveguide (SIW) cavity with a rectangular microstrip patch containing strategically placed slots to enhance bandwidth and radiation performance. As shown in Figs. 4a–c, the design employs a multilayer structure in which the SIW cavity improves isolation and suppresses surface wave losses, while the slotted patch enables multiresonant operation. Figure 4a presents the 3D SIW structure, where two periodic rows of vias form the waveguide sidewalls, confining the electromagnetic fields and guiding energy toward the radiating slots.

The top view of the antenna, consisting of a rectangular patch with three slots and a tapered microstrip feed (dimensions W_f, L_f, W_{f1}, L_{f1}), is illustrated in Fig. 4b. The tapered feed provides improved impedance matching, allowing efficient coupling into the patch, which radiates through two longitudinal and one transverse slots designed to support dual-band operation.

The SIW structure, shown in Fig. 4c, consists of two rows of plated through-hole vias that form effective electrical sidewalls within the substrate, enabling stable antenna performance. The SIW is implemented using 0.5-mm diameter vias as detailed in Tab. 1. A 3.5 × 0.37 mm feedline and a 9.0 × 0.7 mm tapered section excite the 18.4 × 7.5 mm radiating patch.

To enhance gain and impedance matching, three slots are etched onto the patch, including two of the longitudinal (9 × 0.70 mm and 7.72 × 0.70 mm) and one of the transverse (3.10 × 0.70 mm) variety, modifying the current distribution and improving return loss.

For a rectangular dielectric-filled waveguide supporting the dominant TE_{10} mode, the dielectric-filled waveguide width a_d is [19]:

$$a_d = \frac{a}{\sqrt{\varepsilon_r}}\,, \tag{1}$$

where a is the effective width of the waveguide and ε_r is the relative dielectric constant.

The effective width of the SIW a_s is determined by [20]:

$$a_s = a_d + \frac{d^2}{0.98\,p}\,, \tag{2}$$

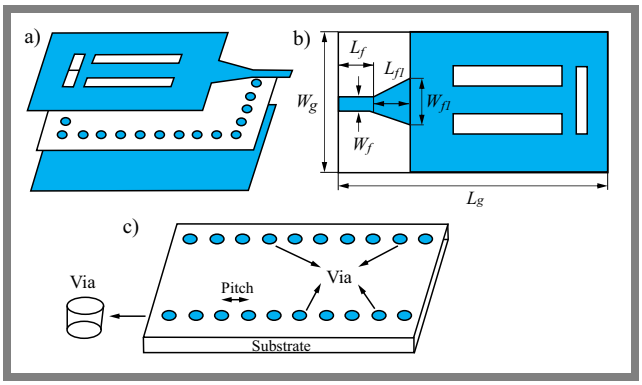

Fig. 4. Layout of the proposed slotted SIW antenna: a) 3D perspective, b) planar surface configuration, and c) internal SIW implementation.

where d is the diameter of the vias in the SIW and p is the pitch or center-to-center distance between the adjacent vias in the SIW structure.

2.3. Parametric Analysis

The slot dimensions affect the impedance matching and resonance frequency of the proposed SIW microstrip antenna, as shown in Figs. 5a–c. For the first longitudinal slot, S-parameter analysis with lengths $L_1 = 7.82 - 8.84$ mm and widths $W_1 = 0.66 - 0.72$ mm found an optimal configuration at $L_1 = 7.9$ mm and $W_1 = 0.7$ mm, achieving reflection coefficients of –46.294 and –53.813 dB at 28 and 38 GHz, respectively.

The transversal slot exhibited stable resonance at 28 GHz across dimension variations, whereas the 38 GHz band experienced minor shifts. The best performance was obtained at $L_2 \times W_2 = 3.1 \times 0.7$ mm. Similarly, the second longitudinal slot provided optimal reflection with $L_3 = 7.72$ mm and $W_3 = 0.7$ mm, highlighting strong sensitivity to slot geometry.

The diameter of the vias plays an important role in determining the resonance frequencies, reflection coefficients, and bandwidth performance of the antenna. Extensive testing of various via diameters revealed three significant configurations relevant to target frequencies. As shown in Fig. 5d, the optimal performance was achieved with a via diameter of 0.5 mm, providing the best resonance characteristics.

On the contrary, a diameter of 0.4 mm through the tube produced resonances at 27.23 and 36.98 GHz, with reflection coefficients of 25.88 and –22.36 dB, respectively. The largest

Tab. 1. Optimized dimension of the slotted SIW antenna.

Parameter	Optimized value [mm]	Parameter	Optimized value [mm]
W_g	7.50	W_1	0.70
L_g	27.00	L_2	3.10
d	0.50	W_2	0.70
W_f	0.37	L_3	7.72
L_f	3.50	W_3	0.70
L_1	9.00	p	1.00

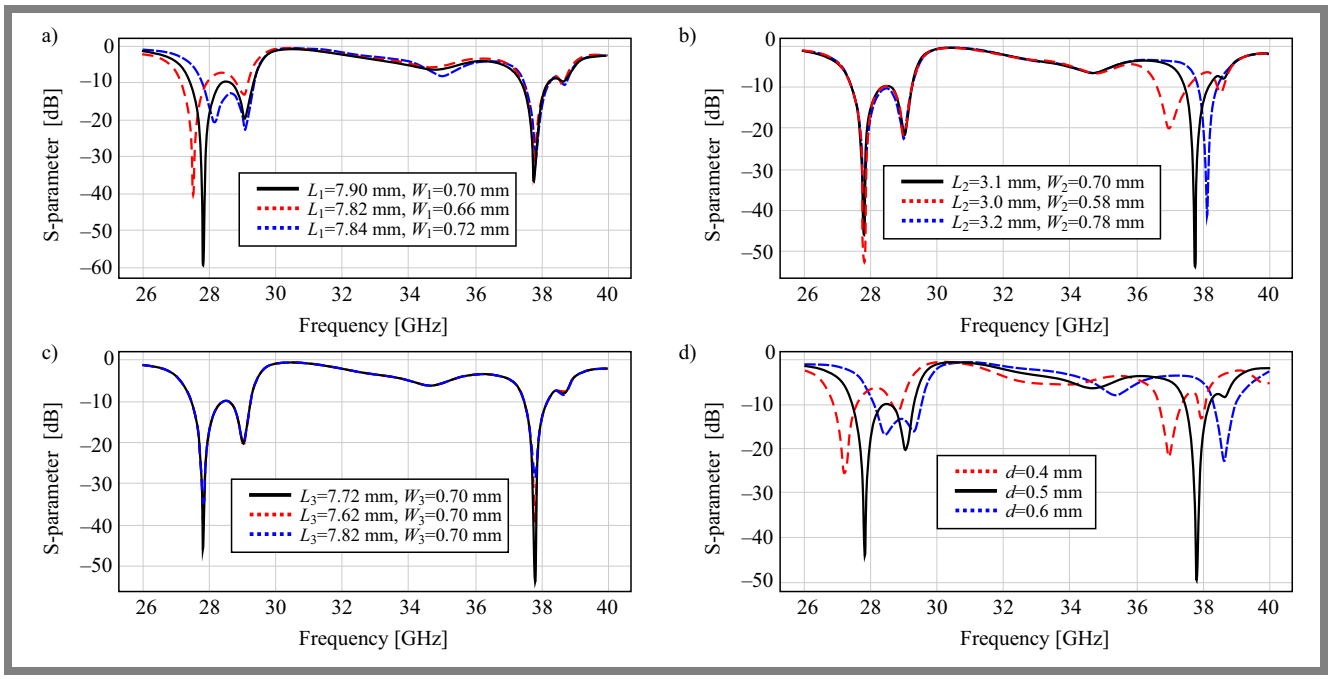

Fig. 5. Results of the parametric analysis of varying lengths and widths of a) the first longitudinal slot (L_1, W_1), b) the transverse slot (L_2, W_2), and c) the second longitudinal slot (L_3, W_3).

diameter tested equaled 0.6 mm and resulted in resonance frequencies deviating from the intended targets, highlighting sensitivity of the antenna's performance to via dimensions.

These CST simulation results serve as a basis for training an ANN model, enabling efficient prediction and optimization of antennas.

3. ANN-based Analysis Method

Conventional full-wave simulations using CST or HFSS software are accurate but computationally expensive, particularly for iterative design. To address this, here, a data-driven ANN model is trained on CST-generated datasets [21], allowing rapid prediction of metrics such as gain and efficiency at 28 and 38 GHz.

ANN effectively captures non-linear dependencies between design parameters and performance outcomes, offering high precision in complex dual-band scenarios [22]. This unified prediction framework streamlines analysis, supports inverse design, and significantly accelerates antenna development [23].

3.1. Data Analysis

As shown in Tab. 2, the data set comprises 158 antenna configurations characterized by 16 parameters, including eight input features such as slot lengths and widths, through diameter, and feedline width, along with eight output metrics (gain and efficiency) for dual-band operation at 28 and 38 GHz. This data set forms the foundation for training the proposed ANN model, enabling it to learn the complex non-linear relationships between antenna geometry and performance.

By varying geometrical and resonance-related parameters during CST-based simulations, a diverse and comprehensive dataset is obtained, capturing realistic design scenarios for dual-band operation. Consequently, the ANN is exposed to underlying physical behaviors and interdependencies that govern antenna gain and efficiency.

3.2. ANN Model Architecture and Training Process

For development, training, and evaluation of an ANN model, eleven pivotal geometrical and resonance-related features, including slot dimensions, through diameter, feeding width, and frequency-dependent parameters, are used as inputs to ensure accurate performance prediction across both bands. The ANN architecture comprises an input layer with 64 neurons processing normalized design features, two hidden layers with 32 and 16 neurons using ReLU activation to capture non-linear relationships, and an output layer that simulta-

Tab. 2. Characteristics of the dataset and model parameters.

Parameter	Description	Description
Dataset size	158 samples	Generated using parametric sweep
Training/test data	126 training (80%), 32 validation/testing (20%)	Ensures proper model generalization
Inputs (dimensions)	8 parameters: $L_1, W_1, L_2, W_2, L_3, W_3, d, W_f$	Used as regression model and ANN inputs
Performance metrics (outputs)	8 metrics: $F_1, F_2, RL_1, RL_2, G_1, G_2, E_{f1}, E_{f2}$	Model prediction targets: frequency, return loss, gain, radiation efficiency

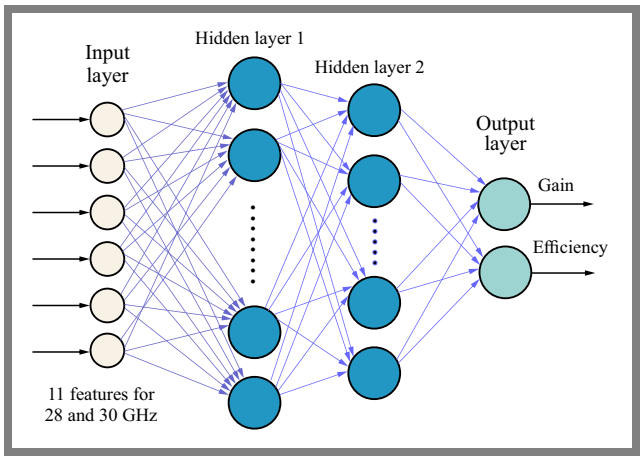

Fig. 6. ANN architecture for the proposed model.

neously predicts gain and efficiency at both frequencies, as shown in Fig. 6. This approach provides a fast and reliable alternative to full-wave electromagnetic simulations for antenna performance evaluation.

The ANN was trained using the Adam optimizer due to its adaptive learning rate and robustness in handling sparse gradients. Hyperparameter tuning identified an optimal learning rate of 0.001, a batch size of 128, and 100 training epochs, which together ensured stable convergence and good generalization performance. The mean squared error (MSE) was used as the loss function, as it effectively penalizes large prediction deviations in this regression task.

As shown in Tab. 2, the generated data set is relatively small, which increases the risk of overfitting. To address potential overfitting and ensure that the ANN model generalizes well, the following strategies were applied:

- The data set was divided into training, validation, and test sets. Model performance was monitored in the validation set to prevent fitting too closely to the training data.
- Techniques such as L2 weight regularization (and/or dropout, if applicable) were used to penalize overly complex models and reduce reliance on any single neuron.
- Training was halted when the validation error stopped improving, preventing unnecessary training epochs that could lead to overfitting.
- The network architecture (number of hidden layers and neurons) was kept as simple as possible while maintaining high predictive performance.
- K-fold cross-validation was employed to evaluate the generalization capability of the ANN by training and validating the model across multiple data partitions, ensuring that all samples contributed to both learning and testing.

This approach provides a more reliable performance estimate and reduces the risk of overfitting, particularly when working with a limited dataset size.

3.3. Model Performance Analysis Method for ANN

To evaluate the performance of the proposed ANN model, standard regression metrics are used, including mean squared error (MSE), mean absolute error (MAE), and root mean squared error (RMSE). These metrics assess predictive accuracy for antenna gain and efficiency at 28 and 38 GHz. MSE, used as the loss function during model training, measures the average squared difference between predicted and actual values [24]:

$$\mathrm{MSE} = \frac{1}{n}\sum_{i=1}^{n}(\hat{y}_i - y_i)^2 \,. \tag{3}$$

MAE provides the mean absolute prediction error:

$$\mathrm{MAE} = \frac{1}{n}\sum_{i=1}^{n}|\hat{y}_i - y_i| \,. \tag{4}$$

RMSE, the square root of MSE, expresses the error in the same units as the target variable [25]:

$$\mathrm{RMSE} = \sqrt{\mathrm{MSE}} = \sqrt{\frac{1}{n}\sum_{i=1}^{n}(\hat{y}_i - y_i)^2} \,, \tag{5}$$

where $\hat{y}_i$ and y_i denote the predicted and actual values, respectively, and n is the number of samples.

These metrics are computed separately for gain and efficiency in both frequency bands, enabling the evaluation of the model's performance.

4. Results and Discussion

4.1. CST Simulation Results

The proposed antenna S-parameter response presented in Fig. 7a shows dual-band operation between 26 and 40 GHz with resonances at 27.83 and 37.81 GHz. At these frequencies, the S_{11} values fall below –10 dB, indicating good impedance matching, with minimum reflection coefficients of –46.29 and –53.82 dB, respectively. Using the –10 dB criterion, the antenna achieves a bandwidth of 1.786 GHz (FBW = 6.41%) at 28 GHz and 0.692 GHz at 38 GHz, confirming its suitability for 5G applications.

The VSWR characteristics provided in Fig. 7b further verify strong matching at the two resonances, where VSWR approaches 1, while a pronounced mismatch peak is observed near 30 GHz. Overall, the antenna demonstrates efficient dual-band performance with superior matching at the two operating frequencies.

Figure 7c illustrates the real and imaginary impedance characteristics of the proposed antenna over 26 – 40 GHz. The real part exhibits strong peaks near 32, 34, and 36.5 GHz, with the 32-GHz peak exceeding 800 Ω, indicating poor matching. Optimal impedance matching occurs at 27.83 and 37.81 GHz, where the real part is minimized and the imaginary part crosses zero, confirming the resonance.

The imaginary component alternates between inductive and capacitive regions, with a pronounced capacitive-type dip at 32 GHz coinciding with the large resistance peak. These impedance features align with the measured VSWR response, validating efficient dual-band operation at the target frequencies.

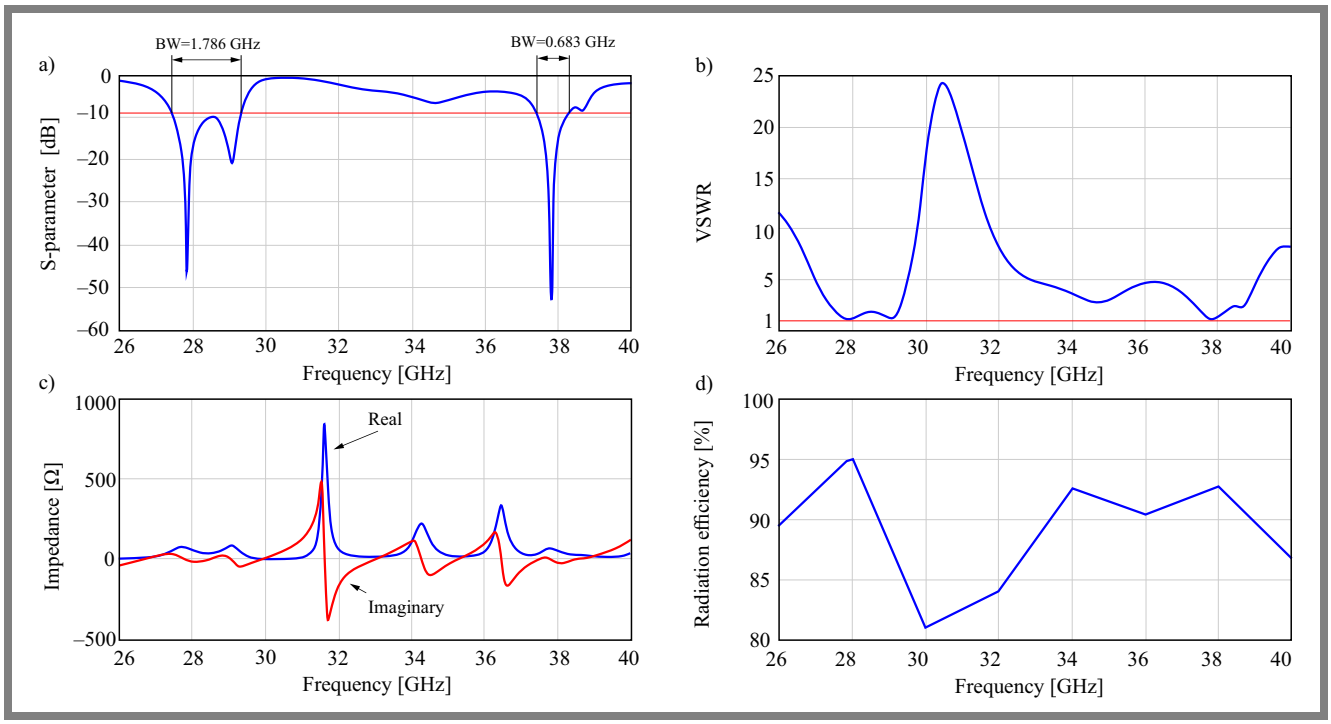

Fig. 7. Analysis of performance metrics for slotted SIW antenna: a) S-parameter, b) VSWR, c) impedance, and d) radiation efficiency.

Figure 7d shows that the proposed SIW antenna achieves excellent radiation efficiency at 26 – 40 GHz, exceeding 90% over the majority of the band. Peak efficiencies of approximately 95% occur at resonant frequencies of 27.83 and 37.81 GHz, indicating highly effective radiation. A slight reduction to approximately 85% is observed near 30 GHz, consistent with the impedance mismatch in this region. In general, the antenna maintains a stable efficiency range of 85 – 95%, demonstrating the low-loss performance of the SIW structure for millimeter wave 5G applications.

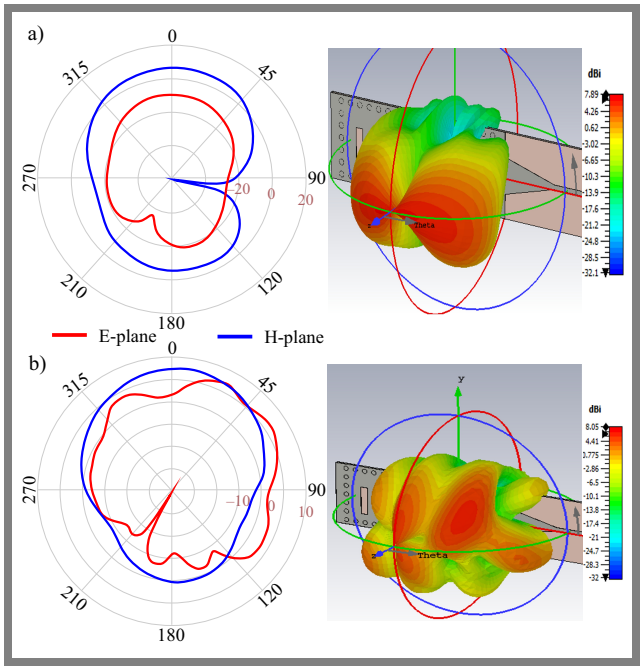

Fig. 8. Gain of the proposed slotted SIW antenna presented using polar and 3D views at: a) 27.83 GHz and b) 37.81 GHz.

For the proposed SIW antenna, simulated radiation patterns at 27.83 and 37.81 GHz (Fig. 8) exhibit quasi-omnidirectional behavior in the E-plane with minimal distortion (3 dB variation) and more directive H-plane patterns with well-defined main and side lobes. This hybrid behavior provides sectoral coverage with controlled elevation beamwidth, suitable for 5G base stations and spatial multiplexing.

The 3D radiation patterns show multilobed structures, with peak gains of 7.89 dB at 27.83 GHz and 8.05 dB at 37.81 GHz. At 37.81 GHz, the radiation is more symmetrical and uniform, with smaller additional lobes that improve multidirectional coverage, demonstrating the effectiveness for mmWave 5G applications.

Tab. 3. Evaluation values of the model test data for 28 and 38 GHz.

Band	28 GHz	38 GHz
Test loss (MSE)	0.032069	0.058893
Test (MAE)	0.120953	0.145232

Tab. 4. MAE, MSE, and RMSE values for 28 and 38 GHz.

Metrics	MAE	MSE	RMSE
Gain (28 GHz)	0.011	0.000	0.016
Efficiency (28 GHz)	0.089	0.014	0.120
Gain (38 GHz)	0.040	0.003	0.055
Efficiency (38 GHz)	0.138	0.051	0.226

Tab. 5. Simulated and predicted gain for the 28 GHz band using the ANN model.

No.	Simulated	Predicted	Error [%]
1	7.931	7.93	0.01
2	7.891	7.89	0.01
3	7.897	7.89	0.09
4	7.891	7.89	0.01
5	7.987	7.98	0.09
6	7.895	7.89	0.06
7	7.900	7.90	0.00
8	7.915	7.92	0.06
9	7.550	7.55	0.00
10	7.595	7.60	0.07

Tab. 6. Simulated and predicted radiation efficiency for the 28 GHz band using an ANN model.

No.	Simulated	Predicted	Error [%]
1	97.17	97.17	0.00
2	97.23	97.17	0.06
3	97.15	97.17	0.02
4	96.69	96.62	0.07
5	96.66	96.64	0.03
6	97.28	97.30	0.02
7	96.51	96.47	0.04
8	96.46	96.46	0.00
9	97.14	97.06	0.08
10	96.83	96.80	0.03

4.2. ANN Prediction Result of Model Performance

This subsection presents the performance of the ANN model to predict gain and efficiency at 28 and 38 GHz. Tables 3 and 4 summarize the evaluation metrics, showing strong overall predictive accuracy. For the 28 GHz band, the MSE and MAE are 0.0321 and 0.121, respectively, while for 38 GHz, they are slightly higher, at 0.0589 and 0.145. Detailed results per output indicate that gain prediction at 28 GHz is highly accurate (MAE 0.011, RMSE 0.016), compared to 38 GHz (MAE 0.040, RMSE 0.055). Efficiency predictions follow a similar trend, with 28 GHz achieving lower errors (MAE 0.089, RMSE 0.120) than 38 GHz (MAE 0.138, RMSE 0.226). Overall, the ANN model performs better at 28 GHz, likely due to differences in the complexity or signal characteristics between the bands.

Figures 9 and 10 present the actual vs. predicted values graphs, illustrating the performance of the ANN model in predicting gain and efficiency at 28 GHz. The predicted values (blue points) closely follow the ideal-fit line (red), indicating strong agreement with the actual targets. The tight clustering around the ideal line for both metrics demonstrates the model's capability to accurately capture complex patterns in multi-output regression tasks. These results validate the reliability and precision of the solution, enabling efficient optimization of antenna parameters while significantly reducing the need for time-consuming full-wave simulations.

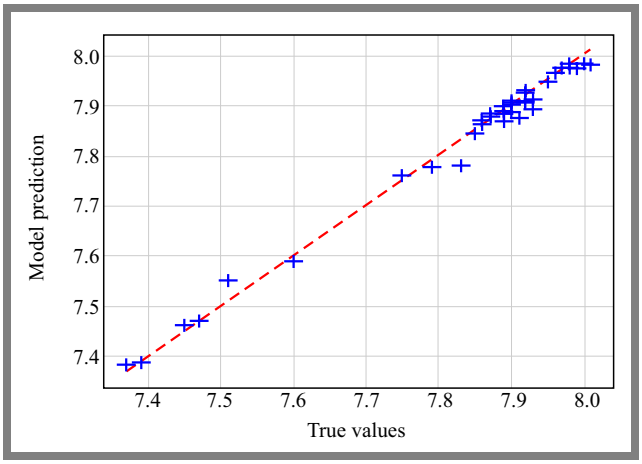

Fig. 9. Actual vs. predicted gain 28 GHz using the ANN model.

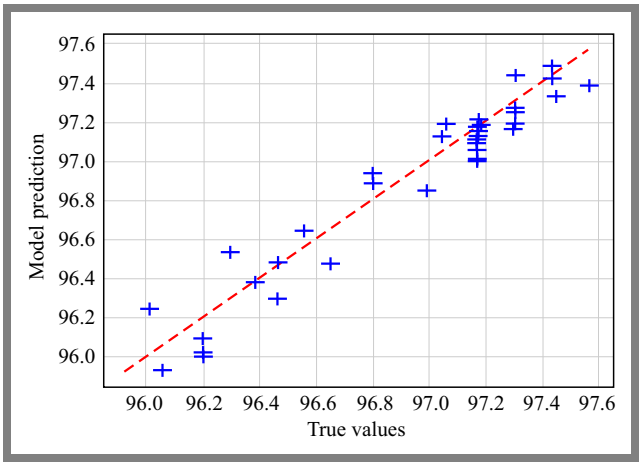

Fig. 10. Actual vs. predicted efficiency 28 GHz using the ANN model.

Tab. 7. Estimation of computational time for different processes.

Process	Approx. time
Single CST simulation	10 – 20 min
Dataset generation (158 samples)	26 – 52 hours
ANN training (100 epochs)	Few minutes
ANN prediction (per sample)	< 1 ms

4.3. ANN-based Validation of Gain

ANN-based gain validation confirms the model's exceptional predictive accuracy with minimal deviation between simulated and predicted values in the 28 and 38 GHz frequency bands. Table 5 provides a comparison between the simulated and predicted gain values across ten samples. At 28 GHz, the ANN demonstrates exceptionally high precision, with error percentages ranging from 0.00% to 0.09% and most predictions deviating by less than 0.06%. This near-perfect

Tab. 8. Performance comparison of the proposed design with related works, using 28/38 GHz antennas.

Ref.	OFB [GHz]	RL [dB]	BW [GHz]	Gain [dB]	Type	Advantages	Limitations	ANN/ML
[26]	28 / 38	–26 / –24	0.9 / 2	9 / 5.9	H-shaped slotted MIMO	High gain (28 GHz), wide bandwidth (38 GHz)	Complex design, low gain (28 GHz)	No
[27]	28 / 38	–19 / –20.75	0.5 / 0.79	12.7 / 15.5	SIW four-element array	Wide bandwidth	Lower reflection coefficient, narrow bandwidth	No
[28]	28 / 38	–17.35 / –34.4	0.982 / 0.354	7.05 / 8.32	Slotted SIW	Compact, simple, high gain (38 GHz)	Lower reflection coefficient, narrow bandwidth	No
[29]	28 / 38	–34.5 / –27.3	1.23 / 1.06	6.6 / 5.86	2-port MIMO	Wide bandwidth	Lower gain	No
[30]	28 / 38	–40 / –52	3 / 3.2	6.8 / 5	4-element MIMO	Wide bandwidth, higher reflection coefficient	Complex design, lower gain	No
[31]	28 / 38	–30 / –40	3.05 / 2.41	8.14 / 8.04	4-element MIMO	Wide bandwidth, higher reflection coefficient, high gain	Complex design, extended simulation times	No
[32]	28 / 38	–33 / –51	0.6 / 0.6	7.4 / 8.1	4-port MIMO	High gain, higher reflection coefficient	Narrow bandwidth	No
[33]	28 / 38	–45 / –45	4.5 / 2.4	4.5 / 7	Circular dual band MIMO	Wide bandwidth, higher reflection coefficient	Complex design, lower gain	ANN
[34]	28	–59.29	0.658	7.63	Patch antenna	Higher reflection coefficient and radiation efficiency	Single band, narrow bandwidth	ML
This work	28 / 38	–46.29 / –53.82	1.786 / 0.683	7.9 / 8.05	Slotted SIW	Simple, higher reflection coefficient, wide bandwidth (28 GHz), high gain	–	ANN

alignment illustrates the strong learning and generalization capability of the model for this band. In contrast, the 38-GHz band also shows reliable performance, though with slightly higher error margins. Prediction errors vary between 0.0127% and 0.244%, with an average still well within acceptable limits. Although still accurate, the slightly increased error in this band may stem from more significant variability or complexity in the electromagnetic characteristic at higher frequencies. Overall, the results confirm that the ANN model is highly capable of emulating CST simulation results with decent accuracy, particularly for the 28 GHz band.

4.4. ANN-based Radiation Efficiency

The ANN validation of radiation efficiency demonstrates excellent predictive accuracy, with strong correlation and close agreement between predicted results and CST simulation data across both frequency bands. As shown in Tab. 6, at 28 GHz, the model demonstrates exceptional accuracy, with prediction errors ranging from 0.00% to only 0.08%, providing an almost perfect match with the simulation results.

For the 38 GHz band, while maintaining impressive overall accuracy, the prediction errors show a modest increase, with deviations typically below 0.1%, but occasionally reaching up to 0.61% in isolated cases. This slight performance difference can be attributed to the inherently more complex electromagnetic interactions at higher frequencies, where smaller physical variations and increased sensitivity to geometric tolerances can influence efficiency characteristics. The low error percentages across both bands, with many predictions deviating less than 0.1% from the simulation results, confirm the robust generalizability of the ANN model.

5. Runtime Performance Comparison

Full-wave electromagnetic simulations using CST Studio Suite software are computationally expensive, particularly for parametric sweeps involving multiple geometrical variables. During the generation of the 158-antenna configuration dataset in CST, the average simulation time was approximately 10 – 20 min on a standard PC. In contrast, once trained, the proposed ANN model predicts antenna gain and radiation efficiency within milliseconds, allowing a near-instantaneous evaluation of new design candidates (Tab. 7).

Although the ANN training process requires an upfront computational cost, this expense is incurred only once. For subsequent optimization and parametric exploration, the ANN-based approach offers a significant increase in speed compared to repeated CST simulations. Therefore, the proposed ANN framework is particularly advantageous for iterative antenna optimization, sensitivity analysis, and inverse design, where hundreds or thousands of evaluations are required.

6. Comparison with Other Works

At operating frequencies of 28 and 38 GHz, the proposed antenna achieves bandwidths of 1.786 GHz and 0.683 GHz, respectively, surpassing most ANN/ML-based designs such as [34], though the results are slightly narrower than in [33], which incurs trade-offs in gain and complexity (Tab. 8). Its

reflection coefficient performance is exceptional, with values of –46.29 dB and –53.82 dB at the respective frequencies, indicating superior impedance matching and minimal signal loss. The antenna demonstrates strong gain performance across both bands, achieving 7.9 dB at 28 GHz and 8.05 dB at 38 GHz, outperforming several referenced designs, including [28]–[30], [33].

At 28 GHz, it remains competitive with high-gain designs such as [32], [33], while slightly trailing [31]. At 38 GHz, the proposed design outperforms the designs proposed in [26], [29], [30], matches the performance of [32] and competes effectively with [29]. Although it is less efficient than specialized arrays in [27], it offers a compact, high-performing, and well-balanced solution with significantly reduced design complexity.

The simple slotted SIW architecture provides advantages over multi-element MIMO configurations, such as [22], [31], making it suitable for compact, densely integrated deployment scenarios. Among machine learning-optimized designs like [33], [34], this work uniquely combines ANN-based optimization with decent performance across all important parameters without compromising simplicity.

7. Conclusions

This work presents the design and optimization of a compact dual-band slotted SIW antenna operating at 28 and 38 GHz, for 5G applications using CST full-wave simulations integrated with a hybrid AI-based framework combining artificial neural networks and polynomial regression. The developed predictive model demonstrated excellent agreement with electromagnetic simulations, achieving prediction errors below 0.1%, which confirms the high precision and reliability of the proposed approach. Moreover, the AI-assisted framework significantly reduced computational burden, enabling performance predictions within 2 to 3 s per model. This represents a reduction of several orders of magnitude in the computation time compared to conventional CST simulations, highlighting the effectiveness of the proposed methodology for rapid and efficient millimeter-wave antenna design.

Acknowledgments

The authors thank Universiti Malaysia Pahang Al-Sultan Abdullah for providing access to laboratory facilities and financial support under Internal Research Grant RDU220382.

References

[1] B. Kaur *et al.*, "Internet of Things (IoT) Security Dataset Evolution: Challenges and Future Directions", *Internet of Things*, vol. 22, art. no. 100780, 2023 (https://doi.org/10.1016/j.iot.2023.100780).

[2] N. Hussain *et al.*, "A Metasurface-based Low-profile Wideband Circularly Polarized Patch Antenna for 5G Millimeter-wave Systems", *IEEE Access*, vol. 8, pp. 22127–22135, 2020 (https://doi.org/10.1109/ACCESS.2020.2969964).

[3] B.A. Esmail and S. Koziel, "Design and Optimization of Metamaterial-based Dual-band 28/38 GHz 5G MIMO Antenna with Modified Ground for Isolation and Bandwidth Improvement", *IEEE Antennas and Wireless Propagation Letters*, vol. 22, pp. 1069–1073, 2022 (https://doi.org/10.1109/LAWP.2022.3232622).

[4] S.K. Hinga and A.A. Atayero, "Deterministic 5G mmWave Large-scale 3D Path Loss Model for Lagos Island, Nigeria", *IEEE Access*, vol. 9, pp. 134270–134288, 2021 (https://doi.org/10.1109/ACCESS.2021.3114771).

[5] J. Lu, G. Huang, D. Hu, and W. Kuai, "Multi-path Data Transmission System Based on 5G Communication Technology", *Journal of ICT Standardization*, vol. 12, no. 1, pp. 71-94, 2024.

[6] N.S. Khair *et al.*, "Recent Advances and Open Challenges in RFID Antenna Applications", *Enabling Industry 4.0 through Advances in Mechatronics*, vol. 900, pp. 507–517, 2022 (https://doi.org/10.1007/978-981-19-2095-0_43).

[7] B. Qian, X. Chen, and A.A. Kishk, "Decoupling of Microstrip Antennas with Defected Ground Structure Using the Common/differential Mode Theory", *IEEE Anten. and Wireless Prop. Lett.*, vol. 20, pp. 828–832, 2021 (https://doi.org/10.1109/LAWP.2021.3064972).

[8] B.S. Bari *et al.*, "Performance Comparison of Early Breast Cancer Detection Precision Using AI and Ultra-wideband (UWB) Bio-antennas", *Proc. of Conference on Cyber Security and Computer Science*, pp. 354–365, 2020 (https://doi.org/10.1007/978-3-030-52856-0_28).

[9] L.H. Xu *et al.*, "Bandwidth Enhancement of the Millimeter-wave Microstrip Linear Array with Loading of Shorting Pins", *IEEE Transactions on Antennas and Propagation*, vol. 71, pp. 1105–1110, 2022 (https://doi.org/10.1109/TAP.2022.3211398).

[10] B. Cheng and Z. Du, "A Wideband Low-profile Microstrip MIMO Antenna for 5G Mobile Phones", *IEEE Transactions on Antennas and Propagation*, vol. 70, pp. 1476–1481, 2021 (https://doi.org/10.1109/TAP.2021.3111330).

[11] M.M. Alam *et al.*, "Design and Optimization of II-shaped Slotted Dual-band SIW Antenna for 5G Applications", *Applications of Modelling and Simulation*, vol. 9, pp. 92–106, 2025.

[12] D. Prabhakar, P. Karunakar, S.R. Rao, and K. Srinivas, "Prediction of Microstrip Antenna Dimension Using Optimized Auto-metric Graph Neural Network", *Intelligent Systems with Applications*, vol. 21, art. no. 200326, 2024 (https://doi.org/10.1016/j.iswa.2024.200326).

[13] P. Kontou, S.B. Smida, and D.E. Anagnostou, "Contactless Respiration Monitoring Using Wi-Fi and Artificial Neural Network Detection Method", *IEEE Journal of Biomedical and Health Informatics*, vol. 28, pp. 1297–1308, 2023 (https://doi.org/10.1109/JBHI.2023.3337001).

[14] M.A. Haque *et al.*, "Machine Learning-based Approach for Bandwidth and Frequency Prediction for N77 band 5G Antenna", *Physica Scripta*, vol. 99, art. no. 026005, 2024 (https://doi.org/10.1088/1402-4896/ad1d40).

[15] H. Ibn-Khedher *et al.*, "Next-generation Edge Computing Assisted Autonomous Driving Based Artificial Intelligence Algorithms", *IEEE Access*, vol. 10, pp. 53987–54001, 2022 (https://doi.org/10.1109/ACCESS.2022.3174548).

[16] M.M. Alam *et al.*, "Machine Learning-based Approach for Bandwidth and Frequency Prediction of Circular SIW Antenna", *Journal of King Saud University–Engineering Sciences*, vol. 37, art. no. 9, 2025 (https://doi.org/10.1007/s44444-025-00010-0).

[17] S. Koziel, A. Pietrenko-Dabrowska, and L. Leifsson, "Antenna Optimization Using Machine Learning with Reduced-dimensionality Surrogates", *Scientific Reports*, vol. 14, art. no. 21567, 2024 (https://doi.org/10.1038/s41598-024-72478-w).

[18] J. Zhang, M.O. Akinsolu, B. Liu, and G.A. Vandenbosch, "Automatic AI-driven Design of Mutual Coupling Reducing Topologies for Frequency Reconfigurable Antenna Arrays", *IEEE Transactions on Antennas and Propagation*, vol. 69, pp. 1831–1836, 2020 (https://doi.org/10.1109/TAP.2020.3012792).

[19] Z. Xu, J. Liu, S. Huang, and Y. Li, "Gain-enhanced SIW Cavity-backed Slot Antenna by Using TE410 Mode Resonance", *AEU – International Journal of Electronics and Communications*, vol. 98, pp. 68–73, 2019 (https://doi.org/10.1016/j.aeue.2018.10.039).

[20] Y. Shi, W.J. Wang, and T.T. Hu, "A Transparent SIW Cavity-based Millimeter-wave Slot Antenna for 5G Communication", *IEEE Antennas and Wireless Propagation Letters*, vol. 21, pp. 1105–1109, 2022 (https://doi.org/10.1109/LAWP.2022.3158418).

[21] R. Olu-Ajayi *et al.*, "Building Energy Consumption Prediction for Residential Buildings Using Deep Learning and Other Machine Learning Techniques", *Journal of Building Engineering*, vol. 45, art. no. 103406, 2022 (https://doi.org/10.1016/j.jobe.2021.103406).

[22] Z.M. Abdhafith, R.A. Ali, and N. Abohmooed, "Impact of Substrate Thickness on the Rectangular Patch Antenna for 5G Communication System by CST Studio", *Wadi Alshatti University Journal of Pure and Applied Sciences*, vol. 2, pp. 79–83, 2024 (https://waujpas.com/index.php/journal/article/view/60/37).

[23] R. Ramasamy and M.A. Bennet, "An Efficient Antenna Parameters Estimation Using Machine Learning Algorithms", *Progress In Electromagnetics Research C*, vol. 130, pp. 169–181, 2023 (https://doi.org/10.2528/PIERC22121004).

[24] D.S.K. Karunasingha, "Root Mean Square Error or Mean Absolute Error? Use their Ratio as Well", *Information Sciences*, vol. 585, pp. 609–629, 2022 (https://doi.org/10.1016/j.ins.2021.11.036).

[25] T.O. Hodson, "Root Mean Square Error (RMSE) or Mean Absolute Error (MAE): When to Use Them or Not", *Geoscientific Model Development*, vol. 15, pp. 5481–5487, 2022 (https://doi.org/10.5194/gmd-15-5481-2022).

[26] P. Liu *et al.*, "Patch Antenna Loaded with Paired Shorting Pins and H-shaped Slot for 28/38 GHz Dual-band MIMO Applications", *IEEE Access*, vol. 8, pp. 23705–23712, 2020 (https://doi.org/10.1109/ACCESS.2020.2964721).

[27] P. Kumawat and S. Joshi, "5G Dual-band Slotted SIW Array Antenna", *Journal of Taibah University for Science*, vol. 15, pp. 321–328, 2021 (https://doi.org/10.1080/16583655.2021.1978830).

[28] J. Singh, F.L. Lohar, and B.S. Sohi, "Design of Dual Band Millimeter Wave Antenna Using SIW Material for 5G Cellular Network Applications", *Materials Today: Proceedings*, vol. 45, pp. 5405–5409, 2021 (https://doi.org/10.1016/j.matpr.2021.02.106).

[29] A.E. Farahat and K.F. Hussein, "Dual-band (28/38 GHz) Wideband MIMO Antenna for 5G Mobile Applications", *IEEE Access*, vol. 10, pp. 32213–32223, 2022 (https://doi.org/10.1109/ACCESS.2022.3160724).

[30] A. Khabba, J. Amadid, S. Ibnyaich, and A. Zeroual, "Pretty-small Four-port Dual-wideband 28/38 GHz MIMO Antenna with Robust Isolation and High Diversity Performance for Millimeter-wave 5G Wireless Systems", *Analog Integrated Circuits and Signal Processing*, vol. 112, pp. 83–102, 2022 (https://doi.org/10.1007/s10470-022-02045-8).

[31] K. Cuneray, N. Akcam, T. Okan, and G.O. Arican, "28/38 GHz Dual-band MIMO Antenna with Wideband and High Gain Properties for 5G Applications", *AEU – International Journal of Electronics and Communications*, vol. 162, art. no. 154553, 2023 (https://doi.org/10.1016/j.aeue.2023.154553).

[32] R.R. Elsharkawy, K.F. Hussein, and A.E. Farahat, "Dual-band (28/38 GHz) Compact MIMO Antenna System for Millimeter-wave Applications", *Journal of Infrared, Millimeter, and Terahertz Waves*, vol. 44, pp. 1016–1037, 2023 (https://doi.org/10.1007/s10762-023-00943-0).

[33] L. Sellak *et al.*, "ANN-based Design of Miniaturized Circular Dual-band 4×4 MIMO Antenna for 28/38 GHz 5G mmWave Applications", *Telkomnika*, vol. 22, pp. 1280–1292, 2024 (https://doi.org/10.12928/telkomnika.v22i5.26347).

[34] S. Md, R. Islam, and S. Sarker, "Machine Learning Based on Patch Antenna Design and Optimization for 5 G Applications at 28 GHz", *Results in Engineering*, vol. 24, art. no. 103366, 2024 (https://doi.org/10.1016/j.rineng.2024.103366).

Md Mahabub Alam, M.Sc.
Faculty of Electrical and Electronics Engineering Technology
https://orcid.org/0009-0005-5036-4608
E-mail: mahbub.ete@gmail.com
Universiti Malaysia Pahang Al-Sultan Abdullah,
Pahang, Malaysia
https://www.umpsa.edu.my

Md Raihanul Islam Tomal, M.Sc.
Faculty of Computing
https://orcid.org/0009-0009-5290-7134
E-mail: raihanultomal@gmail.com
Universiti Malaysia Pahang Al-Sultan Abdullah,
Pahang, Malaysia
https://www.umpsa.edu.my

Ahmad Afif Mohd Faudzi, Ph.D.
Faculty of Electrical and Electronics Engineering Technology
https://orcid.org/0000-0002-3640-5259
E-mail: afif@umpsa.edu.my
Universiti Malaysia Pahang Al-Sultan Abdullah,
Pahang, Malaysia
https://www.umpsa.edu.my

Nurhafizah Abu Talip Yusof, Ph.D.
Faculty of Electrical and Electronics Engineering Technology
Centre for Research in Advanced Fluid and Processes
https://orcid.org/0000-0001-9762-5119
E-mail: hafizahs@umpsa.edu.my
Universiti Malaysia Pahang Al-Sultan Abdullah,
Pahang, Malaysia
https://www.umpsa.edu.my